EARTHQUAKE SPECTRA

The Professional Journal of the Earthquake Engineering Research Institute

PREPRINT

This preprint is a PDF of a manuscript that has been accepted for publication in *Earthquake Spectra*. It is the final version that was uploaded and approved by the author(s). While the paper has been through the usual rigorous peer review process for the Journal, it has not been copyedited, nor have the figures and tables been modified for final publication. Please also note that the paper may refer to online Appendices that are not yet available.

We have posted this preliminary version of the manuscript online in the interest of making the scientific findings available for distribution and citation as quickly as possible following acceptance. However, readers should be aware that the final, published version will look different from this version and may also have some differences in content.

The DOI for this manuscript and the correct format for citing the paper are given at the top of the online (html) abstract.

Once the final, published version of this paper is posted online, it will replace the preliminary version at the specified DOI.

Probabilistic Tsunami Loss Estimation Methodology: Stochastic Earthquake Scenario Approach

Katsuichiro Goda[a] and Raffaele De Risi[a]

This study develops a probabilistic tsunami loss estimation methodology for enhancing community resilience against tsunami disasters. The method is based on novel stochastic earthquake source modeling and state-of-the-art tsunami fragility modeling. It facilitates the quantitative evaluation of tsunami loss for coastal community by accounting for uncertainties of earthquake occurrence and rupture characteristics. A case study is set up to illustrate an application of the developed method to the Sendai Plain area by focusing on possible tsunami events in the Tohoku region of Japan. The quantitative tsunami hazard as well as risk assessment results serve as effective means to make decisions regarding tsunami disaster risk reduction.

INTRODUCTION

A comprehensive risk assessment framework for catastrophic events is a pre-requisite for achieving effective disaster risk reduction and building resilient community against mega-thrust subduction earthquakes (UNISDR 2015). The complex, large-scale nature of cascading risks (e.g. a sequence of mainshock shaking, tsunami, geo-hazard, and numerous aftershocks) causes a great number of fatalities and destroys existing infrastructure, resulting in huge economic loss (Kajitani et al. 2013). To mitigate ground shaking and tsunami risks for coastal community, reliable tools for simulating strong motion and tsunami are needed. To evaluate the impact due to major earthquakes quantitatively, a performance-based earthquake engineering (PBEE) framework was developed by Cornell and Krawinkler (2000), and has been implemented in various studies (e.g. Porter et al. 2006; Goulet et al. 2007). The key ideas for adopting PBEE are to quantify uncertainties associated with individual model components (e.g. hazard, exposure, vulnerability, and loss) and to obtain risk outputs with meaningful estimates of their uncertainties. The framework is particularly useful for defining the long-term objectives in reducing consequences of future natural disasters and for promoting risk-based management decisions (Liel and Deierlein 2013; Yoshikawa and Goda 2014).

As exemplified by recent devastating events in Indonesia, Chile, and Japan, global tsunami exposure is not negligible and coastal communities are vulnerable to infrequent, catastrophic tsunamis

[a] Department of Civil Engineering, University of Bristol, Queen's Building, University Walk, Bristol, BS8 1TR, United Kingdom

(Løvholt et al. 2014). To improve the tsunami preparedness for these locations, integrated tsunami risk mitigation strategies are necessary by combining physical protection measures and emergency response/evacuation measures (FEMA 2008), both of which should be informed by accurate tsunami hazard and risk assessments.

Recent investigations of tsunami impact assessment incorporate the uncertainty associated with earthquake source characteristics (e.g. occurrence, location, magnitude, and fault geometry) through probabilistic tsunami hazard analysis (PTHA; e.g. Geist and Parsons 2006; Burbidge et al. 2008; Horspool et al. 2014). PTHA enables us to identify tsunami source regions and corresponding scenarios that have major impact to a site or region of interest. Moreover, PTHA can be used for the basis of engineering design of coastal structures (e.g. Chock 2016). On the other hand, several stochastic random-field methods have been developed and applied to probabilistic tsunami hazard and risk assessments (Goda et al. 2014; Fukutani et al. 2015; Mueller et al. 2015; Goda and Song 2016). In these methods, slip heterogeneity over the earthquake rupture plane is characterized by wavenumber spectra or some probability density functions, and numerous stochastic source models are generated to assess the variability of the tsunami hazard and risk parameters through Monte Carlo tsunami simulations. Using such stochastic scenario approaches, a set of tsunami inundation hazard maps for coastal cities and towns, corresponding to different tsunami behavior and consequences, can be obtained, which is particularly useful for planning tsunami evacuation and long-term adaptation. At present, integration of PTHA and stochastic scenario approaches has been considered by De Risi and Goda (2016) only, whereas extension of stochastic-scenario-based PTHA to tsunami risk assessment has not been implemented. Such an integrated/extended risk assessment framework can form the fundamental computational framework for performance-based tsunami engineering (PBTE). The above-mentioned method is in sharp contrast with the state-of-the-practice worst credible scenario approach for tsunami hazard mapping (e.g. Cheung et al. 2011) with regard to uncertainty modeling and quantification.

This study presents a novel stochastic-scenario-based tsunami hazard and risk assessment methodology for PBTE. The concept of PBTE is not entirely new (Attary et al. 2017); however, it has not been fully developed nor rigorously implemented in tsunami engineering. Given the similarity and commonality of earthquake and tsunami hazards (i.e. low-probability high-consequence geological events), it is straightforward to apply the PBEE-based mathematical formulation to the tsunami impact assessment (Goda and Song 2016). Indeed, modern PTHA (e.g. Geist and Parsons 2006; Burbidge et al. 2008; Horspool et al. 2014; De Risi and Goda 2016) adopts essentially an identical formulation as probabilistic seismic hazard analysis (PSHA), and such hazard assessment can be extended to probabilistic tsunami risk analysis by incorporating tsunami vulnerability assessment (Wiebe and Cox 2014). One notable difference between earthquake and tsunami hazard-risk analyses

is that typically tsunami simulation is performed by solving the governing equations of wave propagation for given initial conditions of sea surface, unlike the use of statistical ground motion prediction models in seismic hazard-risk analysis. The wave simulation requires more detailed information of earthquake rupture processes, such as heterogeneous earthquake slip and scaling of earthquake characteristics as a function of moment magnitude M_w. Therefore, more accurate estimates of tsunami hazard parameters can be obtained at multiple sites of interest, reducing the uncertainty in hazard components. This also facilitates the realistic and accurate estimation of spatially distributed tsunami hazard parameters (e.g. inundation depth) at building locations, which is different from the seismic hazard counterpart (i.e. spatial correlation models of the ground motion prediction equations are necessary to account for realistic spatial distribution of seismic hazard parameters; see Yoshikawa and Goda 2014). On the other hand, current tsunami vulnerability assessment is largely empirical (Tarbotton et al. 2015; Macabuag et al. 2016), resulting in difficulties when the PBTE framework is applied to geographical regions where empirical tsunami damage data (and thus relevant tsunami fragility models) are lacking. This limitation can be overcome by developing analytical tsunami fragility models (Park et al. 2012; Attary et al. 2016; Petrone et al. 2017), similarly to the seismic vulnerability counterpart. Importantly, one of the goals of this work is to bring both PBEE and PBTE on the coherent computational framework (De Risi and Goda 2016). This will eventually facilitate the development of a performance-based engineering framework for cascading earthquake-tsunami multi-hazards.

To demonstrate the tsunami loss estimation methodology, a case study, focusing upon the Tohoku region of Japan, is presented. The tsunami sources in the off-shore Tohoku region, which correspond to a wide range of earthquake magnitudes from M_w7.5 to M_w9.1, are considered. Note that the set-up of the case study considers near-field sources only and ignores far-field sources; the latter sources may have large influence on the tsunami loss estimation. The uncertainties of the source geometry and rupture characteristics are fully taken into account by using new probabilistic scaling relationships of earthquake source parameters and stochastic synthesis of heterogeneous earthquake slip (Goda et al. 2014, 2016). These uncertainties are propagated through tsunami wave modeling and fragility assessment via Monte Caro simulations. As outputs of the numerical example, single-location as well as spatially-aggregated parameters for multiple locations are considered for tsunami hazard assessment, while tsunami loss to a building portfolio in Natori and Iwanuma Cities is evaluated. Moreover, critical hazard scenarios corresponding to the selected percentiles of the tsunami risk curves (e.g. 1 in 1,000 years tsunami loss event) are derived to demonstrate how additional results can be obtained from the developed stochastic-scenario-based PBTE method.

PROBABILISTIC TSUNAMI LOSS ESTIMATION FRAMEWORK

FORMULATION

A generic equation for probabilistic tsunami risk assessment can be expressed as

$$\nu_L(L \geq l) = \lambda_{Mmin} \int P(L \geq l | ds) f_{DS|IM}(ds|im) f_{IM|S}(im|s) f_{S|M}(s|m) f_M(m) |\mathrm{d}ds \| \mathrm{d}im \| \mathrm{d}s \| \mathrm{d}m| \quad (1)$$

where $\nu_{\boldsymbol{L}}(\boldsymbol{L} \geq l)$ is the mean annual occurrence rate that the tsunami loss $\boldsymbol{L}$ for a portfolio of buildings exceeds a certain loss threshold l. The variables $\boldsymbol{M}$, $\boldsymbol{S}$, $\boldsymbol{IM}$, and $\boldsymbol{DS}$ correspond to earthquake magnitude, earthquake source parameters, tsunami intensity measures, and tsunami damage states, respectively. The integration should be performed over all random variables that are considered in Equation (1).

Moreover, key model components in Equation (1) are defined as follow:

- λ_{Mmin} is the annual occurrence rate of tsunamigenic earthquakes having magnitudes greater than or equal to M_{min}, while $f_{\boldsymbol{M}}$ is the conditional probability distribution of $\boldsymbol{M}$ above M_{min}. A common choice for $f_{\boldsymbol{M}}$ is the truncated Gutenberg-Richter (GR) relationship (Gutenberg and Richter 1956). The earthquake occurrence model shown in Equation (1) is a time-independent Poisson process. A time-dependent renewal model for earthquake occurrence can be incorporated by specifying additional information, i.e. time horizon of the hazard-risk assessment, probability distribution for the inter-arrival time of earthquakes, elapsed time since the last event, and magnitude recurrence model; see Goda and Hong (2006).

- $f_{\boldsymbol{S|M}}$ is the probability density function of $\boldsymbol{S}$ given $\boldsymbol{M}$. The uncertainty associated with variable source characteristics can be represented by probabilistic prediction models of earthquake source parameters and stochastic synthesis of earthquake slip (Goda et al. 2014, 2016).

- $f_{\boldsymbol{IM|S}}$ is the probability density function of $\boldsymbol{IM}$ given $\boldsymbol{S}$, and can be evaluated through tsunami simulations by solving the nonlinear shallow water equations (Goto et al. 1997) for initial boundary conditions of sea surface caused by earthquake rupture (Okada 1985). $\boldsymbol{IM}$ can be obtained for a single location (e.g. water depth and flow velocity) as well as for some extended areas (e.g. inundated area in a city).

- $f_{\boldsymbol{DS|IM}}$ is the tsunami fragility function, which predicts the probability of incurring a particular $\boldsymbol{DS}$ (e.g. collapse and complete damage) for given $\boldsymbol{IM}$. The fragility functions can be derived empirically (De Risi et al. 2017) as well as analytically (Attary et al. 2016; Petrone et al. 2017). When a bivariate fragility model is adopted, $\boldsymbol{IM}$ consists of a vector of multiple intensity values (e.g. depth and velocity). As an alternative to $f_{\boldsymbol{DS|IM}}$, tsunami fragility analysis can be divided into two steps by introducing engineering demand parameters ($\boldsymbol{EDP}$), i.e. $f_{\boldsymbol{DS|IM}} = f_{\boldsymbol{DS|EDP}} \times f_{\boldsymbol{EDP|IM}}$. Such

refinements are particularly relevant for analytical fragility models, as often considered for the PBEE methods (e.g. Porter et al. 2006; Goulet et al. 2007).

- $P(\boldsymbol{L}\geq l|ds)$ is the tsunami loss function given ***DS***, and can be represented by the damage-loss function and the building cost model. A typical tsunami damage-loss function may be specified as a range of loss ratios for given ***DS*** (MLIT 2014); e.g. a complete damage state may correspond to loss ratios between 0.5 and 1.0, expressed as a fraction of the total building replacement cost.

Although all variables in Equation (1), i.e. ***M***, ***S***, ***IM***, and ***DS***, are expressed as continuous random variables, they can be defined and evaluated in a discrete manner. In such cases, integration in Equation (1) should be replaced by summation. It is noteworthy that the target loss variable ***L*** can be defined for a single structure or a building portfolio (which is distributed spatially along the coast). For the latter case, tsunami hazards need to be evaluated over extended areas and vulnerability assessments should be conducted for all assets in the portfolio and for all possible earthquake scenarios. When the fragility and loss model components are omitted (i.e. $f_{\boldsymbol{DS}|\boldsymbol{IM}}$ and $P(\boldsymbol{L}\geq l|ds)$), Equation (1) essentially represents the stochastic-scenario-based PTHA (De Risi and Goda 2016).

In evaluating Equation (1), it is important to choose an efficient ***IM*** such that ***IM*** is highly correlated with ***DS*** or ***EDP*** (Macabuag et al. 2016). From the efficiency viewpoint, momentum flux may be more suitable than inundation depth because it captures the hydrodynamic effects of tsunami waves acting on structures (Park et al. 2017). However, the momentum flux is generally sensitive to grid resolutions and local topographical features, therefore, tsunami simulations should be performed using high-resolution elevation data (10-m or less). Moreover, tsunami fragility models that are based on momentum flux are difficult to validate against observations; thus additional epistemic uncertainty may need to be included in the tsunami risk analysis.

Figure 1 shows the computational procedure for carrying out probabilistic tsunami risk assessment based on stochastic earthquake scenarios. The Monte Carlo simulations are employed to evaluate the tsunami risk equation shown in Equation (1). It is noteworthy that the computational framework shown in Equation (1) and Figure 1 are versatile and therefore, the model components described below can be changed and refined, depending on the specific requirements and constraints of the tsunami impact assessment. More details of the model components for the earthquake occurrence, stochastic earthquake source, tsunami inundation, and tsunami damage-loss, as implemented in this study, are given in the following subsections. The models discussed are developed for the Sendai Plain area in the Tohoku region of Japan, and have been compared with various observations from the 2011 Tohoku tsunami. For instance, sensitivity of offshore and onshore tsunami waves to earthquake ruptures has been investigated by Goda et al. (2014, 2015); their results indicate that stochastic tsunami simulations encompass the observed tsunami inundation and damage during the 2011 Tohoku event. Furthermore, tsunami fragility models that are used in this study have

been developed by De Risi et al. (2017) based on extensive tsunami damage data compiled by the MLIT (2014), whereas assumed building exposure models are consistent with actual building stock and cost information in the Tohoku region. Based on these, developed tsunami risk models are considered to produce realistic results with respect to the 2011 Tohoku tsunami damage and loss.

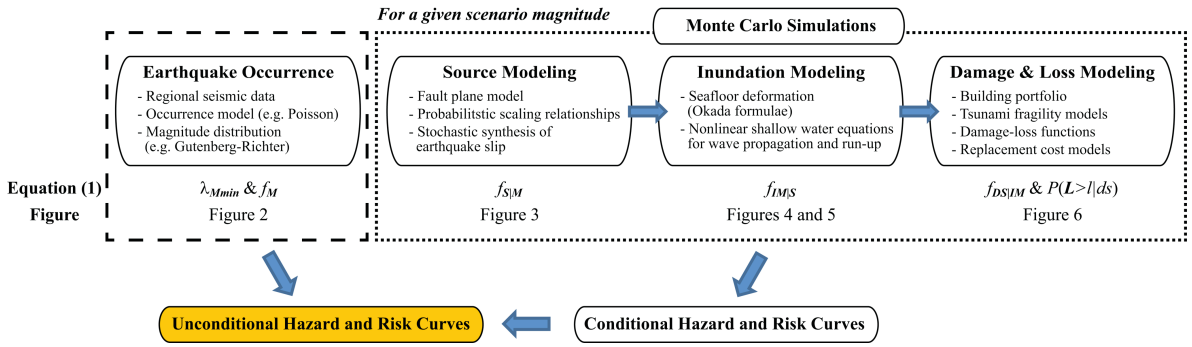

Figure 1. Probabilistic tsunami risk assessment procedure.

EARTHQUAKE OCCURRENCE MODEL

The model components of the earthquake occurrence (i.e. λ_{Mmin} and f_M) can be determined based on the seismicity data in the target region. In this study, the target source region is set to a rectangular zone off the Tohoku region (broken grey line in Figure 2a). This region approximately corresponds to the source zones of off-shore interface subduction earthquakes, which were considered by the Headquarters for Earthquake Research Promotion for the post 2011 Tohoku national seismic hazard assessment (HERP 2013). The HERP seismic hazard model for the Tohoku region is based on a Poisson process, combined with GR magnitude-recurrence models. This is different from other subduction zones in Japan (e.g. Nankai and Tonankai regions), where the renewal-type earthquake occurrence models are adopted. In this study, a set-up similar to the HERP seismic hazard model is considered. It is noteworthy that the above-mentioned model set-up (i.e. adopting GR models with a Poisson occurrence process and estimating model parameters based on short earthquake catalogs) may not produce the reliable estimate of the long-term recurrence rate for large earthquakes (>M8.5) because major historical events are missing in modern instrumental catalogs (e.g. 869 Jogan earthquake for the Tohoku case; see Sawai et al. 2012). The extrapolation of the fitted magnitude-recurrence model should be considered carefully.

The regional seismicity is characterized based on the GR relationship by analyzing seismic data obtained from the Harvard CMT catalog (http://www.globalcmt.org/CMTsearch.html) and the NEIC catalog (http://seisan.ird.nc/USGS/mirror/neic.usgs.gov/neis/epic/code_catalog.html). Figure 2a shows the seismicity data in the offshore Tohoku region from the NEIC catalog. The magnitude-recurrence plots of the earthquake data from the two catalogs are shown in Figure 2b; the GR relationship is fitted to the data by considering the magnitude cut-off of 6. The fitted GR models

indicate that the annual rate of earthquakes with $M \geq 7.5$ can be estimated to be 0.08 per year (i.e. λ_{Mmin}). Note that the fitted GR models shown in Figure 2b are similar to the magnitude-recurrence model adopted by the HERP (2013). Subsequently, the conditional probability distribution function is derived by discretizing the magnitude range that is relevant for tsunami generation triggered by off-shore earthquakes (M7.5 to M9.1) into eight bins with 0.2 interval. This is shown in Figure 2c (i.e. discrete version of f_M). Note that the maximum magnitude is capped at M9.1 and the possibility of having greater magnitudes is neglected.

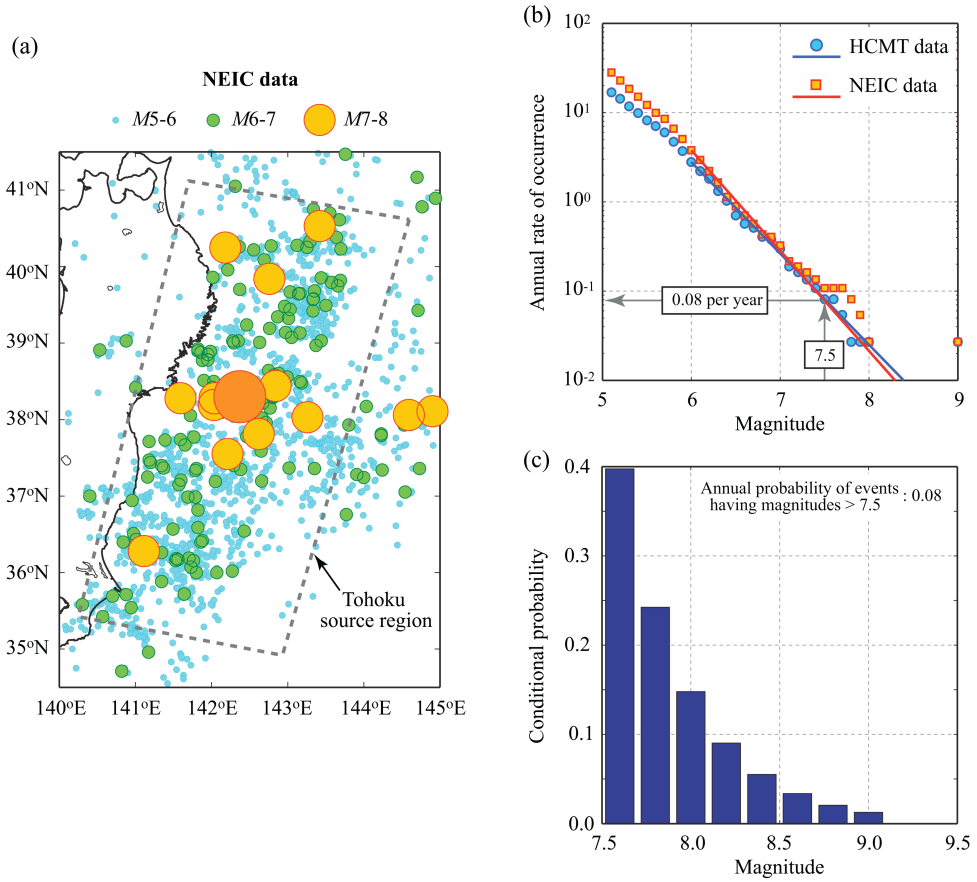

Figure 2. (a) Regional seismicity in the Tohoku region based on the NEIC catalog, (b) Gutenberg-Richter models for the off-shore Tohoku region based on the Harvard-CMT (HCMT) and the NEIC catalogs, and (c) conditional distribution of earthquake magnitude for the off-shore Tohoku region.

EARTHQUAKE SOURCE MODEL

The next step of the tsunami hazard-risk assessment is to generate numerous earthquake source models stochastically (i.e. $f_{S|M}$). It is noted that the approach adopted in this study accounts for uncertainties not only in location and geometry of the fault plane but also in earthquake slip distribution over the rupture plane.

Firstly, the fault model is developed by referring to the rupture plane geometry, such as the top-fault depth, strike, and dip, considered by Satake et al. (2013). The fault model, i.e. extended version

of the Satake et al. fault plane model, covers a 650 km by 250 km area and has a constant strike of 193º along the Japan Trench and variable dip angles, gradually steepening from 8º to 16º along the down-dip direction. The surface projection of the fault plane model is shown as a grey rectangle in Figure 2a. The adopted fault model essentially reflects the current seismological knowledge of earthquake rupture in the target region. To characterize heterogeneous earthquake slip over the fault plane (see below), the source region is discretized into sub-faults having a size of 10 km by 10 km.

Secondly, earthquake source parameters, such as fault width (W), fault length (L), mean slip (D_a), maximum slip (D_m), power transformation parameter for marginal slip distribution (λ), correlation length along dip (A_d), correlation length along strike (A_s), and Hurst number (H), are generated using probabilistic prediction models of these parameters developed by Goda et al. (2016) based on 226 finite-fault models of the past earthquakes. W and L determine the size of the fault rupture as a function of earthquake magnitude. D_a and D_m specify the earthquake slip statistics over the fault plane, whilst λ determines how the slip values are marginally distributed over the fault plane. For example, different values of λ correspond to the normal distribution ($\lambda = 1$, symmetrical bell-shape) and the lognormal distribution ($\lambda = 0$, positively skewed shape). Typically, values of λ fall between 0 and 1 (see Goda et al. [2016] for more details). A_d, A_s, and H are used to characterize the spatial distribution of earthquake slip and are the model parameters for von Kármán wavenumber spectra (Mai and Beroza 2002; Goda et al. 2014). Essentially, the wavenumber spectra specify how slip values are spatially correlated over the fault plane. In evaluating uncertainties (i.e. errors of the prediction equations), correlation of the error terms among different source parameters is taken into account to generate more realistic stochastic earthquake source models. In the simulation, random numbers for the error terms are sampled from the multivariate lognormal distribution.

Thirdly, using the simulated spatial slip distribution parameters (i.e. A_d, A_s, and H), a random slip field is generated using a Fourier integral method (Pardo-Iguzquiza and Chica-Olmo 1993). To achieve slip distribution with realistic positive skewness, the synthesized slip distribution is converted via Box-Cox power transformation using the simulated value of λ. The transformed slip distribution is then adjusted to achieve the target mean slip D_a and to avoid very large slip values exceeding the target maximum slip D_m. Subsequently, the position of the synthesized fault plane is determined randomly within the source region. Due to the uncertainty in the source parameters, random sampling of W, L, and D_a may result in a seismic moment M_o (= μWLD_a where μ is the rock rigidity) that is very different from the target moment magnitude (as specified by the scenario magnitude). To avoid such an inadequate combination of W, L, and D_a, sampling of these three parameters is repeated until the calculated seismic moment falls within a certain range. In this study, the target moment magnitudes minus/plus 0.1 units are considered for such a range (to be consistent with the bin size of

the discretized magnitude distribution, shown in Figure 2c). Further details of the stochastic synthesis can be found in Goda et al. (2014, 2016).

In this study, to capture the uncertain earthquake sources for a given scenario magnitude, 500 stochastic models are generated, and the same procedure is followed for eight magnitude ranges (in total 4,000 source models). The synthesized earthquake source models, which reflect possible variability of tsunami-triggering seismic events in terms of geometry, fault location, and slip distribution, are then used in Monte Carlo tsunami simulations. It is noteworthy that the number of simulated source models (i.e. 500 models) is sufficiently large to obtain stable tsunami hazard results at the sites of interest (see De Risi and Goda [2016]).

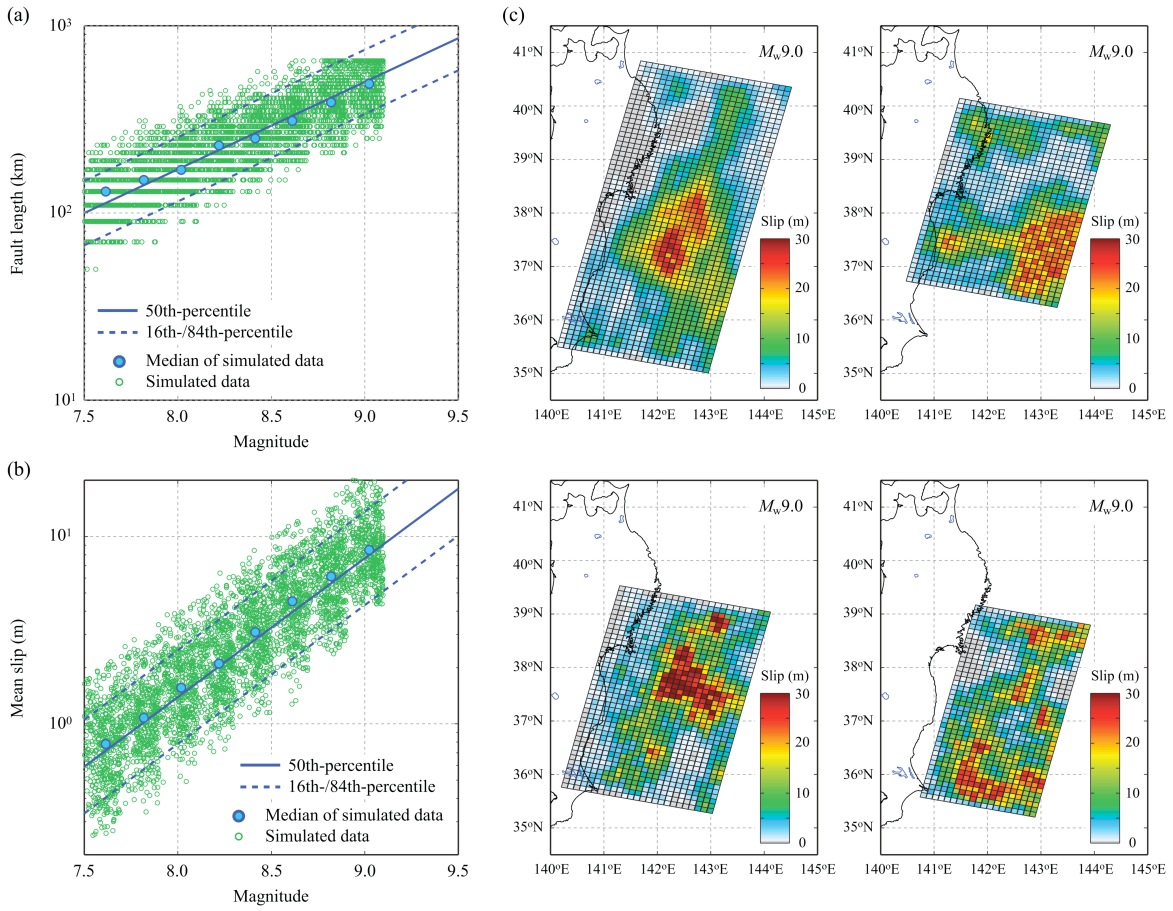

Figure 3. (a,b) Scaling relationships for fault length and mean slip by Goda et al. (2016), in comparison with the simulated fault length and mean slip of the 4,000 stochastic source models, and (c) four realizations of the stochastic source models for the M_w9.0 scenario.

To illustrate the stochastic modeling of earthquake sources, simulated values of the fault length and mean slip of the 4,000 stochastic source models are compared in Figures 3a and 3b, respectively, with the corresponding scaling relationships for the fault length and mean slip by Goda et al. (2016). For the fault length (Figure 3a), it can be observed that the upper limit of 650 km (i.e. maximum length of the target source region) is reached for the M_w9.0 scenario. Due to the trade-off between the fault

length and the mean slip in conserving the total seismic moment, simulated values of the mean slip tend to increase for the M_w9.0 scenario (see Figure 3b). Similarly, sampling of six other source parameters is carried out. Subsequently, based on the simulated source parameters, stochastic synthesis of earthquake slip is performed and the simulated source model is positioned within the target source region. Figure 3c shows four realizations of the synthesized source models for the M_w9.0 scenario. It can be observed that the geometry, location, and slip distribution of the source models vary significantly.

TSUNAMI INUNDATION MODEL

For each of the stochastic source models, tsunami inundation simulation is performed. The initial water surface elevation is evaluated based on formulae by Okada (1985) and Tanioka and Satake (1996). Tsunami wave propagation is evaluated by solving nonlinear shallow water equations with run-up (Goto et al. 1997). The computational domains are nested following a 1/3 ratio rule at four resolutions (i.e. 1350-m, 450-m, 150-m, and 50-m domains). A complete dataset of bathymetry/elevation, coastal/riverside structures, and surface roughness is obtained from the Miyagi Prefectural Government. All bathymetry, elevation, and structural height data are defined with respect to Tokyo Peil, which is the standard mean sea level in Japan. In the tsunami simulation, the coastal/riverside structures are represented by a vertical wall at one or two sides of the computational cells. To evaluate the volume of water that overpasses these walls, Honma's weir formulae are employed (JSCE 2002). The bottom friction is evaluated using Manning's formula following the Japan Society of Civil Engineers standard (JSCE 2002). The fault rupture is assumed to occur instantaneously, and numerical tsunami calculation is performed for duration of 2 hours with an integration time step of 0.5 s. The tidal fluctuation is not taken into account in this study because regional-scale tide models which capture realistic fluctuations at different locations were not available, while the effect of instantaneous ground deformation due to the fault movement is taken into consideration.

For the tsunami hazard and risk assessment in this study, coastal areas of Natori and Iwanuma Cities (the Sendai Plain) are focused upon. The topography of the areas is the low-lying coastal plain; see the elevation map shown in Figure 4. During the 2011 Tohoku tsunami, the areas were inundated completely and the majority of the buildings near the coast were destroyed (Fraser et al. 2013). A zoomed map of Figure 4 shows the spatial distribution of buildings located in Natori and Iwanuma. The building dataset considered in this study is obtained from the Ministry of Land Infrastructure and Transportation (MLIT 2014). The building dataset contains 6,791 low-rise structures (1 to 4 stories), consisting of three structural/material types, i.e. reinforced concrete (RC), steel, and wood. The number of RC, steel and wooden structures is 137, 558, and 6,096, respectively, and the majority of the buildings in Natori and Iwanuma are residential. To discuss the tsunami hazard results at a single

location later, three points A to C are selected along the coastal line. The water depths at Points A and C (in sea) are 2 m, while the elevation at Point B (inland) is 3.9 m above mean sea level.

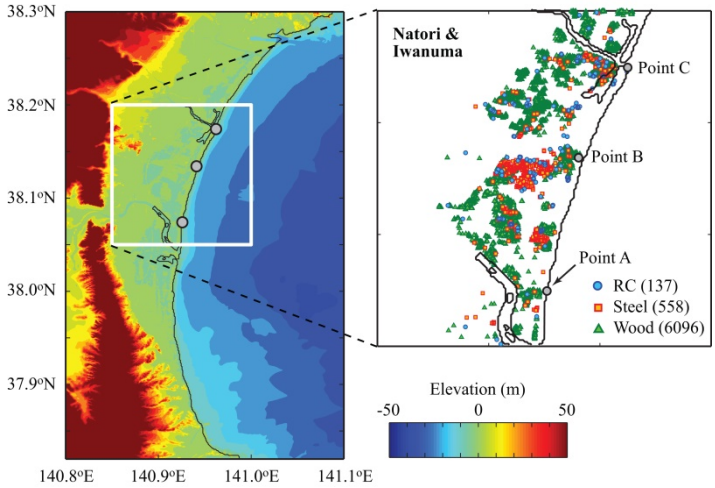

Figure 4. Elevation model and building portfolio in Natori and Iwanuma Cities, the Sendai Plain, Japan.

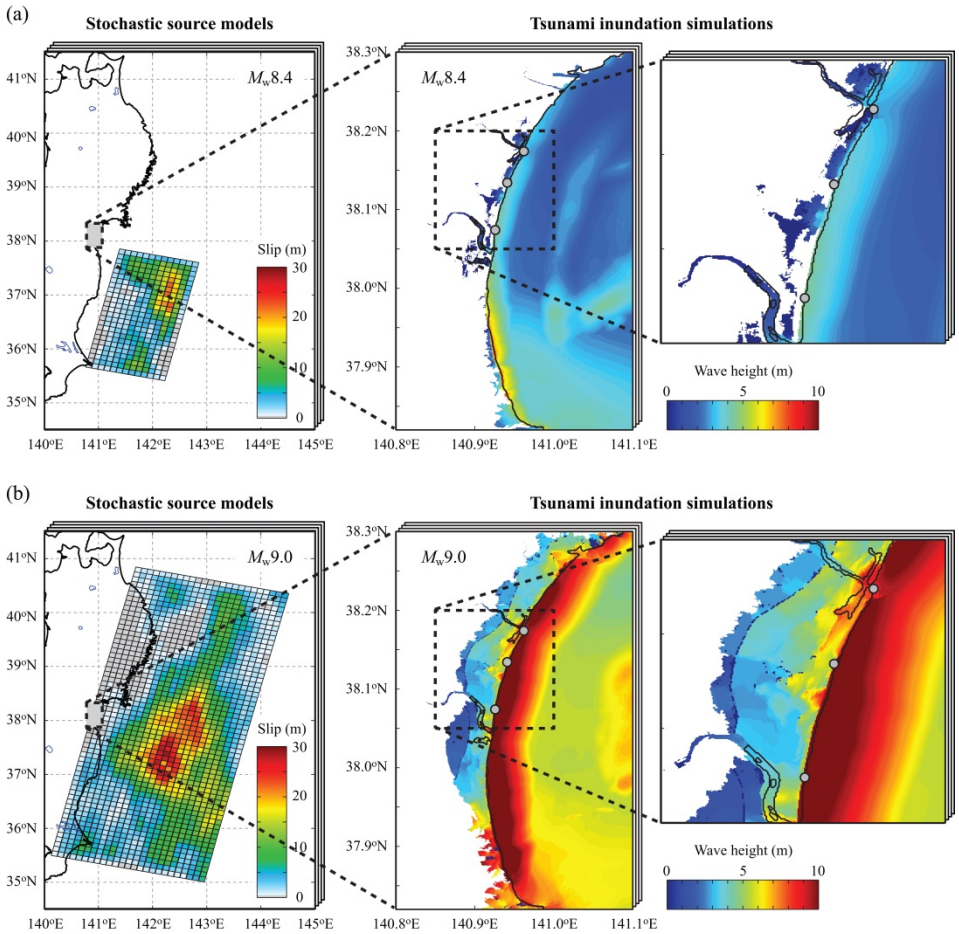

Figure 5. Stochastic earthquake source models and tsunami inundation results: (a) M_w8.4 scenario and (b) M_w9.0 scenario.

Figure 5 illustrates the Monte Carlo tsunami simulations for two stochastic sources (M_w8.4 and M_w9.0 events). For different magnitude scenarios, tsunami inundation simulations are conducted in the areas of interest, and relevant tsunami hazard parameters (e.g. maximum wave height and depth) are obtained. Using the inundation maps, spatially-aggregated tsunami hazard parameters, such as inundation areas above a certain depth, can be calculated. Subsequently, the computed tsunami hazard parameters (i.e. ***IM***) are used for evaluating tsunami fragility and damage (i.e. ***DS***). Although the results shown in Figure 5 are two specific examples, it can be observed that greater earthquake magnitude results in significant increase of the rupture area as well as the earthquake slip amplitude (as characterized by the scaling relationships; see Figures 3a and 3b). Consequently, the extent of tsunami inundation increases significantly with the earthquake magnitude. More comprehensive results based on numerous source models will be discussed later.

BUILDING PORTFOLIO AND TSUNAMI DAMAGE-LOSS ESTIMATION

To evaluate the tsunami damage (i.e. $f_{\boldsymbol{DS|IM}}$), for each tsunami simulation, tsunami fragility models developed by De Risi et al. (2017) are applied. Figure 6a compares two sets of tsunami fragility models for five tsunami damage states (i.e. minor, moderate, extensive, complete, and collapse) for RC buildings and wooden buildings, respectively (note: the fragility models for steel buildings typically lie between those for RC and wooden buildings; see De Risi et al. [2017]). The damage states are defined by the MLIT (2014), which conducted extensive tsunami damage surveys after the 2011 Tohoku tsunami. These fragility models have been developed based on the tsunami damage data from the 2011 Tohoku tsunami and thus are consistent with the building exposure data shown in Figure 4. The input parameters for the fragility models are inundation depths at building locations and material/structural type of the buildings. It is noted that the fragility models developed by Der Risi et al. (2017) can utilize the additional information on flow velocity to improve the tsunami damage estimation. Such vector-***IM*** fragility models are not used in this study because spatial grid resolutions of the bathymetry and elevation data used in tsunami simulations are at 50 m, which may be too crude to estimate the flow velocity at building locations accurately.

After applying the fragility models and taking differences of the estimated exceedance probabilities for two adjacent damage states, discrete probabilities can be obtained for minor, moderate, extensive, complete, and collapse damage states. Subsequently, for each structure, a random number from the standard uniform distribution is generated and is compared with the damage state probabilities. This determines the realized damage state for this structure during the considered tsunami event. Each damage state is associated with a range of loss ratios. More specifically, loss ratio ranges for minor, moderate, extensive, complete, and collapse damage states are defined as 0.0–0.1, 0.1–0.3, 0.3–0.5, 0.5–1.0, and 1.0 (deterministic), respectively. The uniform distribution is

assumed for the loss ratios. Note that the loss ratios are applied to the total cost of a building (see below), which includes both structural and non-structural elements.

By sampling the total buildings cost of stores/offices and houses (Figure 6b), which is considered to be lognormally distributed, the tsunami damage cost can be estimated (i.e. $P(\boldsymbol{L} \geq l|ds)$). The Monte Carlo sampling is repeated for all structures and earthquake scenarios. The building cost models shown in Figure 6b are estimated based on two sources of information: unit building cost statistics and floor area statistics. The mean and coefficient of variation (CoV) of the unit replacement costs are obtained from the Japanese building cost information handbook published by the Construction Research Institute (2011). Using the cost handbook, mean unit cost = 1,500 US$/m^2 and CoV = 0.33 are adopted for stores/offices, whereas mean unit cost = 1,600 US$/m^2 and CoV = 0.33 are adopted for wooden houses (note: 1 US$ = 100 yen). The adopted cost statistics are for the Tohoku region. Moreover, typical floor areas of stores/offices and wooden houses are determined based on the national construction statistics maintained by the MLIT (http://www.mlit.go.jp/toukeijouhou/chojou/stat-e.htm). In this study, floor areas of 540 m^2 and 130 m^2 are adopted for stores/offices and wooden houses, respectively, by averaging the construction data for Miyagi and Iwate Prefectures during the period between 2012 and 2014. The floor areas are considered to be lognormally distributed with CoV = 0.33. Based on the above building cost information, the expected total cost of the 6,791 buildings is 1830.9 million US$.

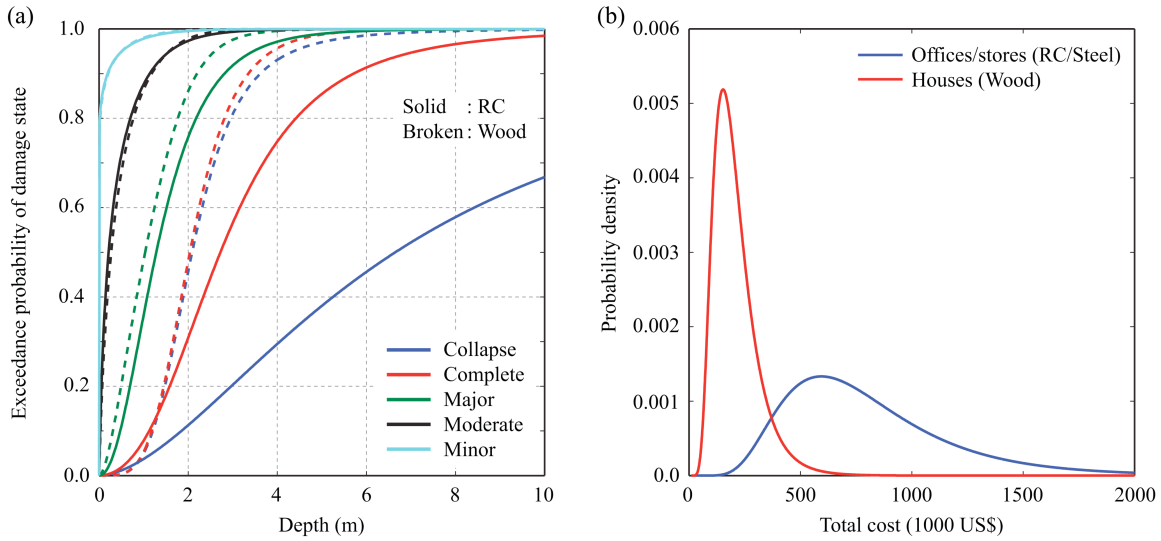

Figure 6. (a) Tsunami fragility curves for RC and wooden structures and (b) probabilistic models for the total building cost for offices/stores and residential houses.

NUMERICAL EVALUATION OF TSUNAMI RISK EQUATION

As the results of the preceding probabilistic tsunami risk assessment, tsunami loss samples for 6,791 structures are obtained for 4,000 stochastic source models. These loss samples, together with λ_{Mmin} and $f_{\boldsymbol{M}}$, can be used to obtain the tsunami loss exceedance curve for a building portfolio of

interest by evaluating Equation (1) numerically. The calculation step of integrating different components is illustrated in Figure 7. Through Monte Carlo tsunami simulations and tsunami damage-loss analyses, the conditional tsunami loss curve $P(\boldsymbol{L}\geq l|\boldsymbol{M})$ can be evaluated numerically. The results of $P(\boldsymbol{L}\geq l|\boldsymbol{M})$ for four magnitude values are shown in Figure 7a in a form of cumulative distribution function (note: loss results for M_w7.6 to M_w8.2 are omitted intentionally as they are relatively small). It can be observed that the chance of experiencing large tsunami loss increases significantly with the earthquake magnitude. To evaluate the values of $\nu_{\boldsymbol{L}}(\boldsymbol{L}\geq l)$ as a function of loss threshold l (i.e. unconditional tsunami loss curve), $P(\boldsymbol{L}\geq l|\boldsymbol{M})$ can be obtained from the cumulative distribution function – an example of this operation for l = 1,000 million US$ is shown in Figure 7a. Once the conditional exceedance probabilities of tsunami loss are evaluated for all magnitudes, they are weighted by their occurrence probabilities (i.e. λ_{Mmin} and $f_{\boldsymbol{M}}$) and are summed to obtain the unconditional tsunami loss estimate. This calculation step for l = 1,000 million US$ is shown in Figure 7b. By repeating the above procedures for various threshold values, the unconditional tsunami loss distribution (which reflects a range of magnitude scenarios from M7.5 to M9.1) can be obtained. It is noted that these procedures are also applicable to the development of tsunami hazard curves for intensity parameters of interest.

It is important to investigate the effects of the number of simulations (i.e. stochastic sources) per magnitude on the tsunami loss results because the Monte Carlo methods are adopted to evaluate the tsunami risk equation. Figure 8a shows the conditional tsunami loss percentiles (2.5th, 16th, 50th, 84th, and 97.5th) for the M_w9.0 scenario as a function of the simulation number, which is varied from 50 to 500. The results indicate that the conditional tsunami loss curves are stable when a sufficient number of stochastic source models (a few hundreds) are used for the conditional tsunami loss distributions. Although individual results for other scenario magnitudes are not shown, similar conclusions can be obtained, with tendency that tsunami loss percentiles fluctuate more when magnitudes are smaller (but the absolute values of tsunami loss percentiles become smaller at the same time). This trend can be explained by noting that the location of the fault plane with respect to the building portfolio varies more significantly when a smaller scenario magnitude is considered. Moreover, Figure 8b compares the unconditional tsunami loss curves that are obtained based on different numbers of stochastic source models per magnitude. When the number of simulations is relatively small (50 or 100), the tsunami loss curves are more jagged, whilst increasing the number of simulations results in more stable and smooth tsunami loss curves. Overall, it can be concluded that using 4,000 stochastic source models (i.e. 500 rupture cases per magnitude) produces stable tsunami loss results for the tsunami loss estimation conducted in this study.

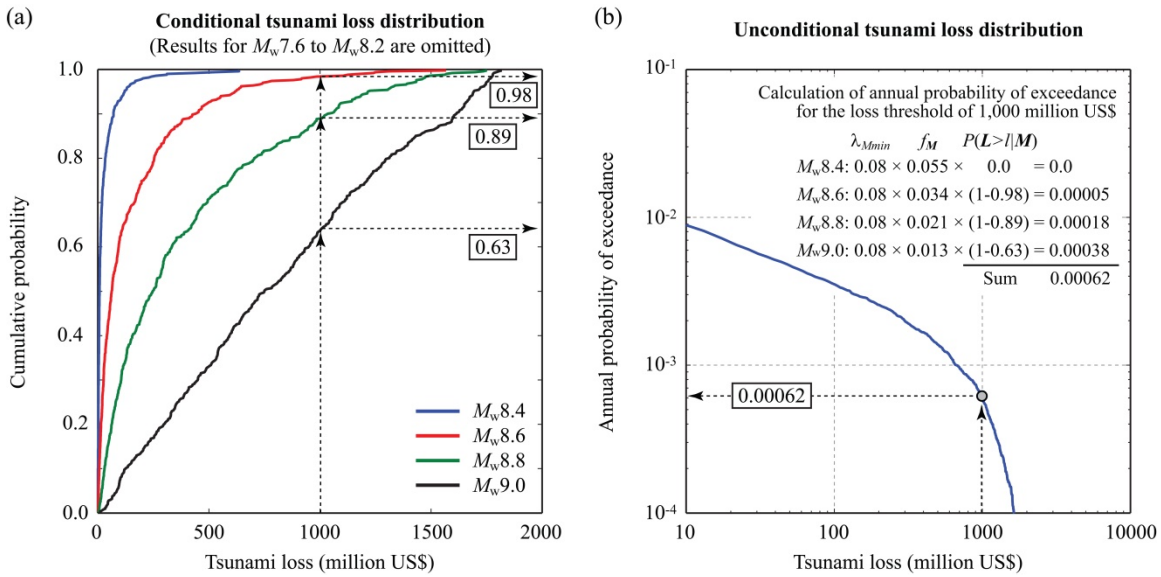

Figure 7. Numerical evaluation of unconditional tsunami loss distribution based on conditional tsunami loss distributions and occurrence probabilities of events having specific scenario magnitudes.

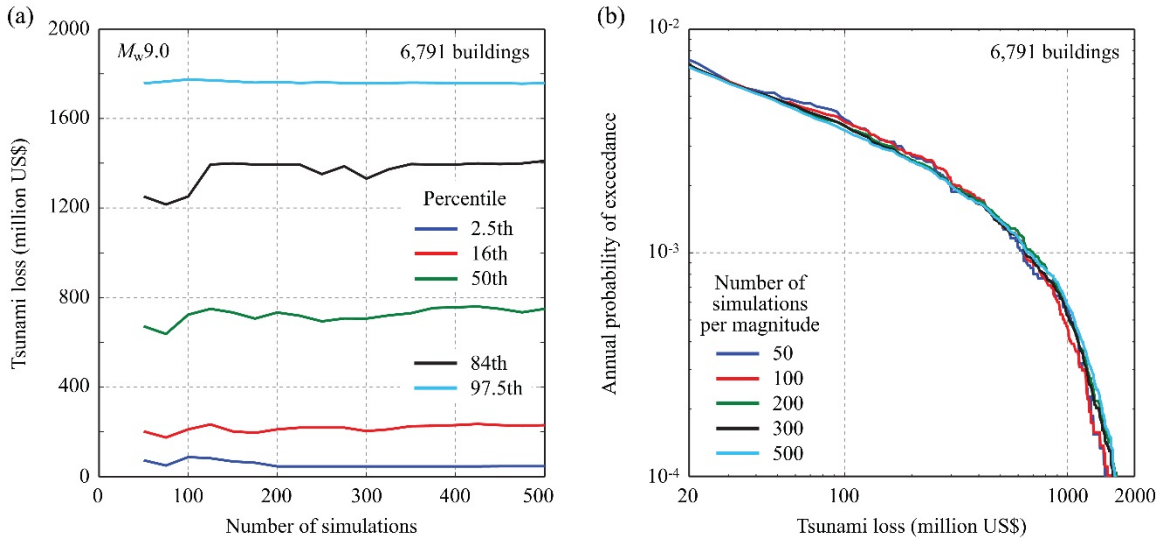

Figure 8. Sensitivity of the tsunami loss estimates to the number of simulations per magnitude: (a) conditional tsunami loss percentiles for the M_w9.0 scenario and (b) unconditional tsunami loss curves.

ILLUSTRATION

In this section, results from the probabilistic tsunami hazard and risk assessments of the buildings in Natori and Iwanuma Cities in the Sendai Plain area are presented. Firstly, tsunami hazard estimates for single locations as well as areas in Natori and Iwanuma are discussed. Secondly, tsunami loss results for the building portfolio located in Natori and Iwanuma are discussed by emphasizing issues related to tsunami risk management.

TSUNAMI HAZARD ANALYSIS

The probabilistic estimates of the maximum tsunami wave height (which is measured from mean sea level) at a near-shore location are the fundamental input for designing coastal structures and developing an effective risk management plan (e.g. Chock 2016). To illustrate the stochastic-scenario-based PTHA, tsunami wave-height hazard curves for Points A to C (see Figure 4) are evaluated and the results are shown in Figure 9. Figure 9a presents the conditional tsunami wave-height hazard curves for Point A, whilst Figure 9b shows the unconditional tsunami wave-height hazard curves for Points A to C. The integration of the conditional hazard curves for different magnitude ranges into the unconditional hazard curve is carried out by following a similar procedure explained in Figure 7 (but focusing on tsunami wave height at a single location, rather than tsunami loss for the building portfolio). The conditional hazard curves for Point A (Figure 9a) clearly show that tsunami intensity increases significantly with the earthquake magnitude (noting that the horizontal axis is logarithmic). The unconditional hazard curve for Point A, shown in Figure 9b, indicates that the expected tsunami wave height for Point A at the 1,000-year return period level reaches 10 m, whereas the corresponding hazard value for Point B is only 6.3 m (note: the differences of the hazard values for Points A and C are mainly attributed to the existence of local tsunami barrier at the mouth of Natori River near Point C). These hazard values may be relevant to engineering design when coastal defense structures are to be constructed at these locations. It can also be seen that the unconditional hazard curve for Point B has a flat part (which is shown with a broken line) – this is because Point B is an onshore site at 3.9 m altitude. Only relatively large earthquakes cause tsunami waves that reach Point B; the annual probability of such inundation events can be estimated to be 0.0034 ≈ 300 years return period.

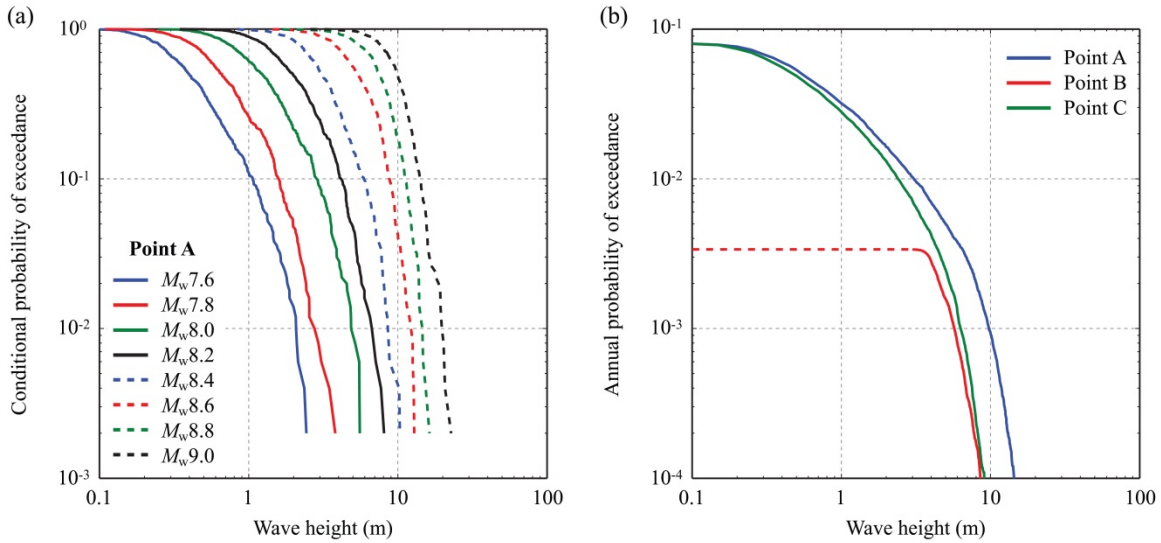

Figure 9. Tsunami wave-height hazard curves: (a) conditional curves for Point A and (b) unconditional curves for Points A, B, and C.

A notable advantage of the proposed stochastic tsunami simulation method is that accurate tsunami inundation modeling is performed; therefore, detailed inundation results for all stochastic source scenarios are available for post-processing. In such a case, inundation areas above a certain depth can be used as tsunami hazard parameters, facilitating tsunami hazard assessment and mapping for seaside areas of cities and towns. To demonstrate this, inundation areas above 1 m, 2 m, 3m, and 5 m depth in Natori and Iwanuma are calculated. Figure 10a shows eight conditional inundation-area hazard curves for the 1 m threshold value, while Figure 10b shows the unconditional inundation-area hazard curves for the four depth threshold values. It is noted that the inundation-area hazards are significantly affected by the local terrain characteristics (e.g. Figure 4). The unconditional hazard curves corresponding to the four depth thresholds indicate that inundation areas at the 1,000-year return period level decrease significantly from about 30 km^2 (1 m depth) to about 2 km^2 (5 m depth). Typically, in the alluvial plain region, inundation areas with large depths are confined to seaside areas along the coast.

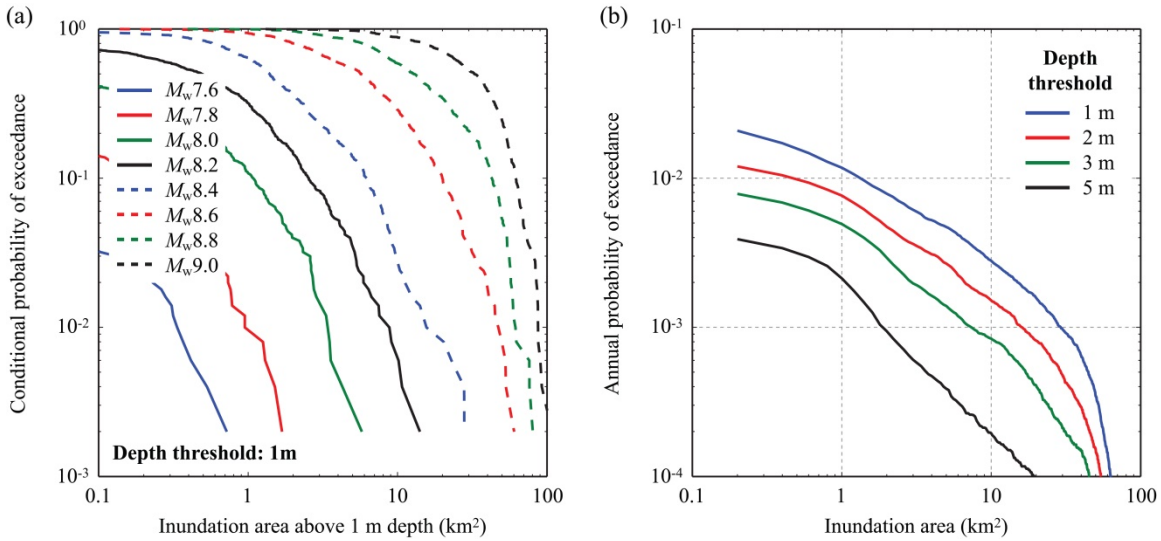

Figure 10. Tsunami inundation-area hazard curves for Natori and Iwanuma: (a) conditional curves for inundation areas above 1 m depth and (b) unconditional curves for inundation areas above 1, 2, 3, and 5 m depth.

Moreover, the Monte Carlo tsunami simulations facilitate the generation of stochastic tsunami wave profiles at locations of interest. Such tsunami wave profiles for Point B are shown in Figure 11 for three magnitude ranges. The tsunami wave profiles shown in Figure 11 are adjusted for land elevation, thus the wave amplitudes correspond to inundation depths, rather than wave heights (as shown in Figure 9b). Note that tsunami flow velocity profiles, although not shown in this study, can be generated, and some other tsunami hazard parameters, such as Froude number and momentum flux, can be evaluated in a similar manner (Macabuag et al. 2016; Petrone et al. 2017). The results shown in Figure 11 highlight that the tsunami wave amplitudes increase significantly with the earthquake magnitude, and that approximately 55 to 60 minutes are available at this location for

evacuation prior to the arrival of major tsunami waves. It is also clear that inspection of the average trend as well as variability of the key tsunami hazard parameters provides valuable insight in developing local tsunami evacuation strategies. From a tsunami engineering perspective, simulated tsunami waveforms are particularly useful for carrying out advanced structural analyses subjected to tsunami wave loading to develop analytical tsunami fragility models (Attary et al. 2016; Petrone et al. 2017).

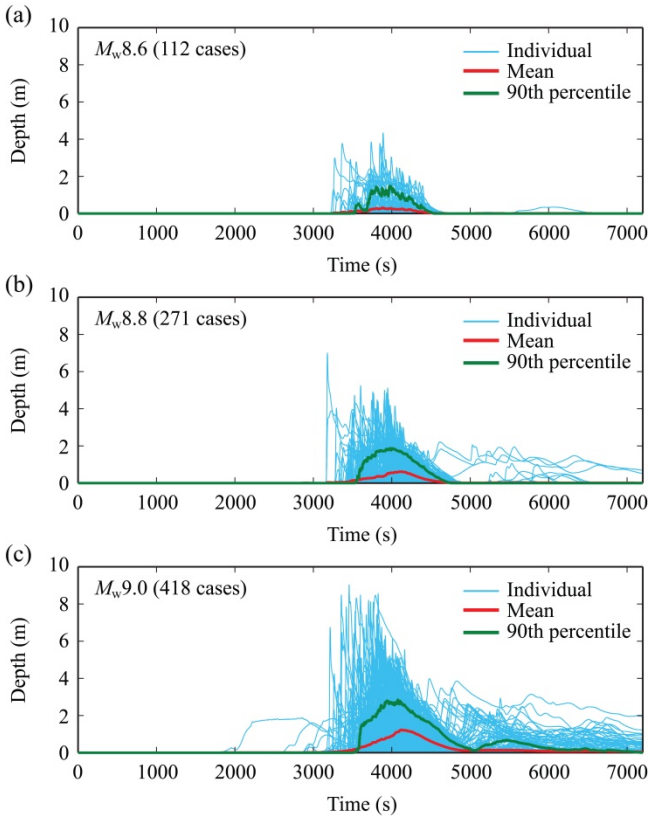

Figure 11. Tsunami wave profiles for Point B (elevation = 3.9 m): (a) M_w8.6 scenario, (b) M_w8.8 scenario, and (c) M_w9.0 scenario.

TSUNAMI LOSS ESTIMATION

As already demonstrated in Figures 7 and 8, the stochastic-scenario-based tsunami risk analysis procedure can be used to obtain a robust estimate of the tsunami loss curve for the building portfolio. It is noteworthy that although detailed results are not shown in this study, similar tsunami loss calculations have been carried out for the entire coast of Miyagi Prefecture; the considered building dataset includes more than 150,000 structures for the tsunami loss estimation. This clearly demonstrates high potential for implementing the developed tsunami risk methodology at regional and national levels. In fact, the most computationally extensive aspects of the method are Monte Carlo tsunami simulations, and the computational efforts required for the tsunami damage and loss assessments are relatively minor.

Figure 12a shows the conditional tsunami loss curves for all buildings in Natori and Iwanuma for the eight magnitude ranges. It can be seen that for extreme cases of the M_w8.8 and M_w9.0 scenarios, the tsunami loss values tend to be saturated because almost all buildings are in the complete damage or collapse damage state. This can happen because the majority of the buildings in Natori and Iwanuma are wooden residential houses (Figure 4), which will be washed away when the tsunami depth exceeds 4 m (Figure 6a). Figure 12b shows the unconditional tsunami loss curves for all buildings as well as three individual building types (RC, steel, and wood). The results shown in Figure 12b indicate that the majority of the tsunami loss in Natori and Iwanuma is concentrated in the residential sector. Figure 12b also provides quantitative information related to the current tsunami risk exposure for the building portfolio. For instance, the expected tsunami losses at the 500 and 1,000 years return period levels are about 300 and 670 million US$, respectively. Although detailed results are not discussed further in this study, various risk metrics, such as annual expected loss (AEL), value at risk (VaR), and tail value at risk (TVaR), which are popular in financial industry, can be computed and used for disaster risk management decisions (Yoshikawa and Goda 2014).

One of the advantages of the proposed tsunami risk assessment method is that tsunami loss results and corresponding tsunami hazard scenarios (in terms of inundation maps as well as earthquake source models) can be related directly. For illustration, two inundation depth maps that correspond to tsunami loss fractiles at the 500 and 1,000 years return period levels are shown in Figure 12c and Figure 12d, respectively. It can be clearly observed that with the increase of the return period level, inundation areas in Natori and Iwanuma increase significantly, thus damaging more buildings in these coastal communities. Importantly, presenting both tsunami loss curves and critical hazard maps will facilitate the risk communication among various stakeholders who have different technical background and capability in understanding probabilistic tsunami risk results and different interests (e.g. expected fatality, financial risk, and tsunami evacuation). Furthermore, from retrospective viewpoints, the tsunami loss curves can be compared with the actual tsunami loss caused by the 2011 Tohoku event. By considering the observed tsunami damage states compiled by the MLIT (2014) and the same information on loss ratio and building cost, the tsunami damage loss for the building portfolio is evaluated as 1,043 million US$. This approximately corresponds to the return period of 1,850 years. Indeed, the observed tsunami inundation areas in Natori and Iwanuma (Goda et al. 2015) are larger than the inundation areas shown in Figure 12d (i.e. 1,000 years return period). These comparisons will be useful for communicating probabilistic tsunami loss results with non-technical stakeholders.

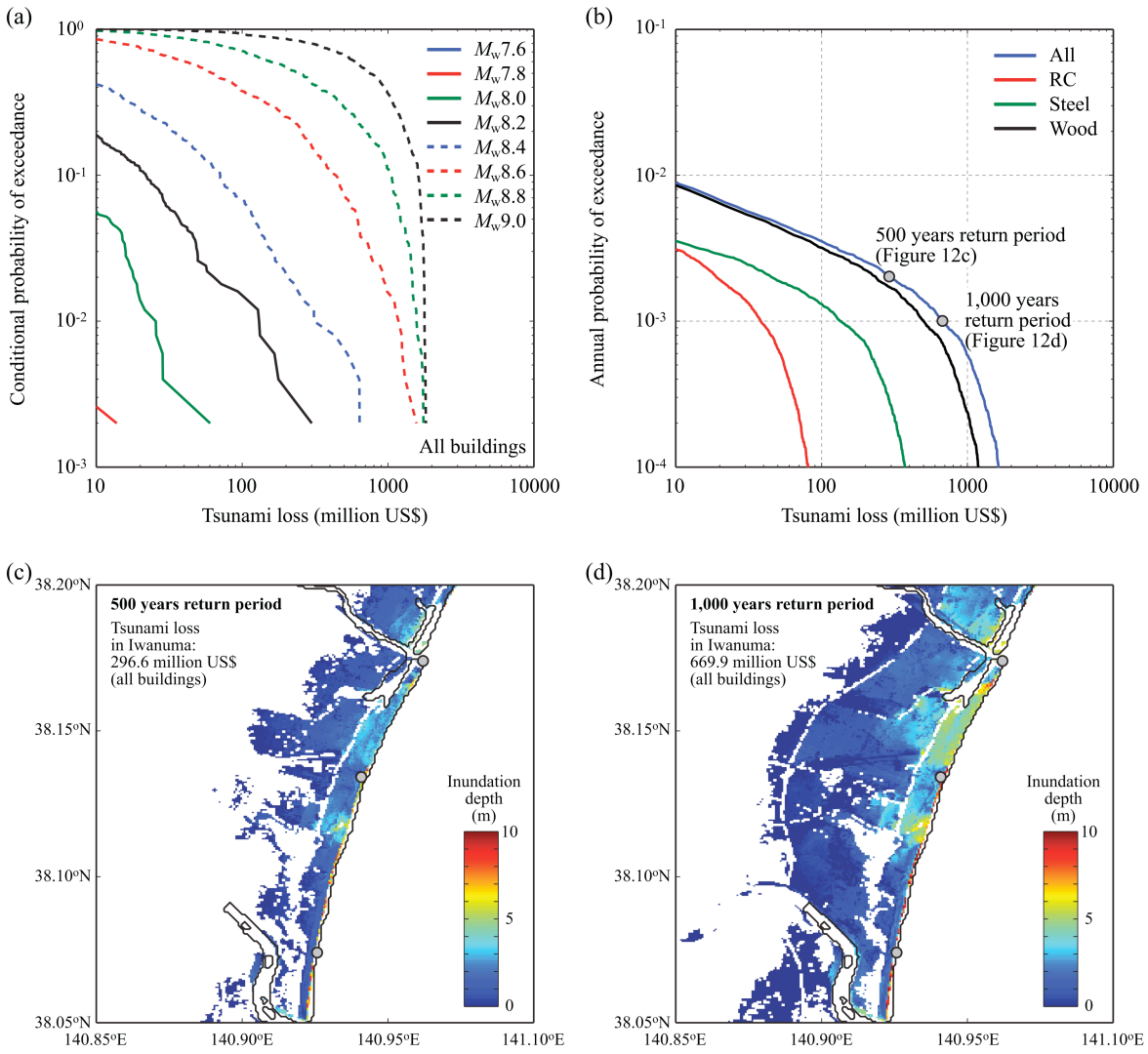

Figure 12. Tsunami loss results for Natori and Iwanuma: (a) conditional loss curves for all buildings, (b) unconditional loss curves for all, RC, steel, and wooden buildings, (c) inundation depth map for the 500 years return period, and (d) inundation depth map for the 1,000 years return period.

As the last remark, although detailed investigations are not carried out in this study, an effective way to utilize the tsunami loss results in tsunami risk management is to perform similar tsunami risk assessments by implementing risk mitigation measures in the numerical models and to compare the loss curves. For instance, heights of tsunami defense structures (e.g. revetments and walls along coast and rivers) may be varied to investigate the cost-effectiveness of the mitigation measures. To achieve such goals, tsunami fragility models for different structural configurations and corresponding cost models are needed. Alternatively, different plans for land use and building zonation can be implemented. Essentially, such investigations will facilitate quantitative cost-benefit analysis of tsunami disaster risk mitigation measures for coastal community.

CONCLUSIONS

This study developed a probabilistic tsunami risk assessment methodology for promoting the performance-based tsunami engineering (PBTE). The method is innovative in that uncertainties associated with earthquake source modeling are fully taken into account by integrating new prediction models of earthquake source parameters and stochastic synthesis of heterogeneous earthquake slip. The uncertainties in tsunami generation are propagated through Monte Carlo tsunami simulations including inland tsunami inundation. This facilitates the generation of various tsunami hazard parameters and outputs at different spatial scales (local, regional, and national). Through the post-processing of the tsunami simulation results and the tsunami fragility analysis, tsunami hazard and loss curves can be derived, which incorporate uncertainties related to earthquake occurrence, earthquake source rupture, tsunami propagation, building damage, and damage cost estimation. Most importantly, the proposed PBTE framework can be used for quantitative cost-benefit analysis of tsunami risk mitigation measures and will promote risk-informed management as well as financial decisions related to tsunami disaster risk reduction. It is also highlighted that the proposed method is compatible with the performance-based earthquake engineering (PBEE), and thus it can be used as the fundamental computational framework for assessing cascading earthquake-tsunami hazards and risks caused by the common earthquake rupture sources in the future.

ACKNOWLEDGEMENTS

This work was supported by the Engineering and Physical Sciences Research Council (EP/M001067/1).

REFERENCES

Attary, N., van de Lindt, J.W., Unnikrishnan, V.U., Barbosa, A.R., and Cox, D.T., 2016. Methodology for development of physics-based tsunami fragilities, *J. Struct. Eng.*, doi: 10.1061/(ASCE)ST.1943-541X.0001715.

Attary, N., Unnikrishnan, V.U., van de Lindt, J.W., Cox, D.T., and Barbosa, A.R., 2017. Performance-Based Tsunami Engineering methodology for risk assessment of structures, *Eng. Struct.* **141**, 676–686.

Burbidge, D., Cummins, P.R., Mleczko, R., and Thio, H.K., 2008. A probabilistic tsunami hazard assessment for Western Australia, *Pure Appl. Geophys*. **165**, 2059–2088.

Cheung, K.F., Wei, Y., Yamazaki, Y., and Yim, S.C., 2011. Modeling of 500-year tsunamis for probabilistic design of coastal infrastructure in the Pacific Northwest, *Coast. Eng.* **58**, 970–985.

Chock, G.Y.K., 2016. Design for tsunami loads and effects in the ASCE 7-16 standard, *J. Struct. Eng.*, 142, 04016093.

Construction Research Institute, 2011. Japan Building Cost Information 2011, Tokyo, Japan, 547 p.

Cornell, C.A., and Krawinkler, H., 2000. Progress and challenges in seismic performance assessment, *PEER Center News* **3**, 4 p.

De Risi, R., and Goda, K., 2016. Probabilistic earthquake–tsunami multi-hazard analysis: application to the Tohoku region, Japan, *Front. Built Environ.* **2**, 25.

De Risi, R., Goda, K., Yasuda, T., and Mori, N., 2017. Is flow velocity important in tsunami empirical fragility modeling?, *Earth-Sci. Rev.* **166**, 64–82.

Federal Emergency Management Agency (FEMA), 2008. Guidelines for design of structures for vertical evacuation from tsunamis, FEMA P646, Washington DC.

Fraser, S., Pomonis, A., Raby, A., Goda, K., Chian, S.C., Macabuag, J., Offord, M., Saito, K., and Sammonds, P., 2013. Tsunami damage to coastal defences and buildings in the March 11th 2011 Mw9.0 Great East Japan earthquake and tsunami, *Bull. Earthq. Eng.* **11**, 205–239.

Fukutani, Y., Suppasri, A., and Imamura, F., 2015. Stochastic analysis and uncertainty assessment of tsunami wave height using a random source parameter model that targets a Tohoku-type earthquake fault, *Stoch. Environ. Res. Risk Assess.* **29**, 1763–1779.

Geist, E.L., and Parsons, T., 2006. Probabilistic analysis of tsunami hazards. *Nat. Haz.* **37**, 277–314.

Goda, K., and Hong, H.P., 2006. Optimal seismic design for limited planning time horizon with detailed seismic hazard information, *Struct. Saf.* **28**, 247–260.

Goda, K., Mai, P.M., Yasuda, T., and Mori, N., 2014. Sensitivity of tsunami wave profiles and inundation simulations to earthquake slip and fault geometry for the 2011 Tohoku earthquake, *Earth Planets Space* **66**, 105.

Goda, K., Li, S., Mori, N., and Yasuda, T., 2015. Probabilistic tsunami damage assessment considering stochastic source models: application to the 2011 Tohoku earthquake, *Coast. Eng. J.* **57**, 1550015.

Goda, K., and Song, J., 2016. Uncertainty modeling and visualization for tsunami ha-ard and risk mapping: a case study for the 2011 Tohoku earthquake, *Stoch. Environ. Res. Risk Assess.* **30**, 2271–2285.

Goda, K., Yasuda, T., Mori, N., and Maruyama, T., 2016. New scaling relationships of earthquake source parameters for stochastic tsunami simulation, *Coast. Eng. J.* **58**, 1650010.

Goto, C., Ogawa, Y., Shuto, N., and Imamura, F., 1997. Numerical method of tsunami simulation with the leap-frog scheme, IOC Manual, UNESCO, No. 35, Paris, France.

Goulet, C.A., Haselton, C.B., Mitrani-Reiser, J., Beck, J.L., Deierlein, G.G., Porter, K.A., and Stewart, J.P., 2007. Evaluation of the seismic performance of a code-conforming reinforced-

concrete frame building - from seismic hazard to collapse safety and economic losses, *Earthq. Eng. Struct. Dyn.* **36**, 1973–1997.

Gutenberg, B., and Richter, C.F., 1956. Magnitude and energy of earthquakes, *Annals Geophys*. **9**, 1–15.

Headquarters for Earthquake Research Promotion (HERP), 2013. Investigations of future seismic hazard assessment, 217 p.

Horspool, N., Pranantyo, I., Griffin, J., Latief, H., Natawidjaja, D.H., Kongko, W., Cipata, A., Bustaman, B., Anugrah, S.D., and Thio, H.K., 2014. A probabilistic tsunami hazard assessment for Indonesia, *Nat. Haz. Earth Sys. Sci.* **14**, 3105–3122.

Japan Society of Civil Engineers (JSCE), 2002. Tsunami assessment method for nuclear power plants in Japan. https://www.jsce.or.jp/committee/ceofnp/Tsunami/eng/JSCE_Tsunami_060519.pdf.

Kajitani, Y., Chang, S.E., and Tatano, H., 2013. Economic impacts of the 2011 Tohoku-Oki earthquake and tsunami, *Earthq. Spectra* **29**, S457–S478.

Liel, A.B., and Deierlein, G.G., 2013. Cost-benefit evaluation of seismic risk mitigation alternatives for older concrete frame buildings, *Earthq. Spectra* **29**, 1391–1411.

Løvholt, F., Glimsdal, S., Harbitz, C.B., Horspool, N., Smebye, H., de Bono, A., and Nadima, F., 2014. Global tsunami hazard and exposure due to large co-seismic slip, *Intl. J. Disaster Risk Red.* **10**, 406–418.

Macabuag, J., Rossetto, T., Ioannou, I., Suppasri, A., Sugawara, D., Adriano, B., Imamura, F., Eames, I., and Koshimura, S., 2016. A proposed methodology for deriving tsunami fragility functions for buildings using optimum intensity measures, *Nat. Haz.* **84**, 1257–1285.

Mai, P.M., and Beroza, G.C., 2002. A spatial random field model to characterize complexity in earthquake slip, *J. Geophys. Res. Solid Earth* **107**, 2308.

Ministry of Land Infrastructure and Transportation (MLIT), 2014. Survey of tsunami damage condition. http://www.mlit.go.jp/toshi/toshi-hukkou-arkaibu.html.

Mueller, C., Power, W., Fraser, S., and Wang, X., 2015. Effects of rupture complexity on local tsunami inundation: Implications for probabilistic tsunami hazard assessment by example, *J. Geophys. Res. Solid Earth* **120**, 488–502.

Okada, Y., 1985. Surface deformation due to shear and tensile faults in a half-space, *Bull. Seismol. Soc. Am.* **75**, 1135–1154.

Pardo-Iguzquiza, E., and Chica-Olmo, M., 1993. The Fourier integral method: an efficient spectral method for simulation of random fields, *Math. Geol.* **25**, 177–217.

Park, P., van de Lindt, J.W., Cox, D., Gupta, R., and Aguiniga, F., 2012. Successive earthquake-tsunami analysis to develop collapse fragilities, *J. Earthq. Eng.* **16**, 851–863.

Park, H., Cox, D.T., and Barbosa, A.R., 2017. Comparison of inundation depth and momentum flux based fragilities for probabilistic tsunami damage assessment and uncertainty analysis, *Coast. Eng.* **122**, 10–26.

Petrone, C., Rossetto, T., and Goda, K., 2017. Fragility assessment of a RC structure under tsunami actions via nonlinear static and dynamic analyses, *Eng. Struct.* **136**, 36–53.

Porter, K.A., Scawthorn, C.R., and Beck, J.L., 2006. Cost-effectiveness of stronger woodframe buildings, *Earthq. Spectr*a **22**, 239–266.

Satake, K., Fujii, Y., Harada, T., and Namegaya, Y., 2013. Time and space distribution of coseismic slip of the 2011 Tohoku earthquake as inferred from tsunami waveform data, *Bull. Seismol. Soc. Am.* **103**, 1473–1492.

Sawai, Y., Namegaya, Y., Okamura, Y., Satake, K., and Shishikura, M., 2012. Challenges of anticipating the 2011 Tohoku earthquake and tsunami using coastal geology, *Geophys. Res. Lett.* **39**, L21309.

Tanioka, Y., and Satake, K., 1996. Tsunami generation by horizontal displacement of ocean bottom, *Geophys. Res. Lett.* **23**, 861–864.

Tarbotton, C., Dall'Osso, F., Dominey-Howes, D. and Goff, J., 2015. The use of empirical vulnerability functions to assess the response of buildings to tsunami impact: comparative review and summary of best practice, *Earth-Sci. Rev.* **142**, 120–134.

United Nations International Strategy for Disaster Reduction (UNISDR), 2015. Sendai Framework for disaster risk reduction, 2015–2030. http://www.unisdr.org/we/coordinate/sendai-framework.

Wiebe, D.M., and Cox, D.T., 2014. Application of fragility curves to estimate building damage and economic loss at a community scale: a case study of Seaside, Oregon, *Nat. Haz.* **71**, 2043–2061.

Yoshikawa, H., and Goda, K., 2014. Financial seismic risk analysis of building portfolios, *Nat. Haz. Rev.* **15**, 112–120.